Crystallization-Based Separation of ε-Caprolactam from a Depolymerization Reaction Mixture – Fundamentals and Potential Separation Strategies

Axel Schultheis, Vico Tenberg, Liisa Rihko-Struckmann, Kai Sundmacher and Heike Lorenz*

DOI: 10.1002/cite.202400120

Dedicated to Prof. Dr.-Ing. Andreas Seidel-Morgenstern on the occasion of his retirement

Depolymerization and subsequent capture of monomers is of interest for process efficiency and sustainability. Polyamide-6 (PA-6) can be depolymerized in aqueous solution using a homogeneous catalyst. To purify the ε-caprolactam (CPL) monomer and recycle the catalyst, two potential crystallization-based strategies are studied: direct crystallization from the reaction mixture and liquid-liquid extraction prior to crystallization. Solubilities in water and promising organic solvents were measured and compared to predictions using perturbed-chain statistical associating fluid theory (PC-SAFT) or conductor-like screening model for real solvents (COSMO-RS). Detailed solid-liquid equilibria (SLE) of the CPL/water system were investigated utilizing DSC and PXRD. This work provides an overview of important factors of PA-6 depolymerization including recycling of tungstophosphoric acid (TPA) and purification of CPL monomers. A first conceptual process design to be further developed is derived.

Keywords: ε-Caprolactam, Crystallization, Depolymerization, Liquid-liquid extraction, Polyamide-6

Received: September 18, 2024; *revised:* October 15, 2024; *accepted:* October 15, 2024

1 Introduction

Recently, depolymerization has become an important approach to tackle the ever-increasing problem of polymer waste and low-valued plastic residues. Pyrolysis, gasification, or catalytic cracking are the established pathways for mixed or contaminated plastic waste [1]. However, the potential chemical products of these thermochemical processes are unspecified, partially water-soluble mixtures of functionalized hydrocarbons or oxygenates. Furthermore, in presence of heteroatoms in the polymer structure, such as nitrogen in polyamides (PA), these thermochemical routes are less favored. An economically feasible depolymerization, i.e., a catalytic recycle process yielding the initial monomer in high quality and quantity, would speed up the transition toward circular economy as multiple monomer → polymerization → use → depolymerization cycles would become conceivable. The various solvolysis processes (e.g., hydrolysis, glycolysis, methanolysis, ammonolysis, or aminolysis) can break ether, ester, and acid amide bonds [1]. The known pathways to depolymerize polyamide-6 (PA-6, or nylon-6) are acidic hydrolysis with phosphoric acid, alkaline hydrolysis with sodium hydroxide, and neutral hydrolysis with subcritical water to yield the monomer, ε-caprolactam (CPL), or alcoholysis with isopropanol to mention a few [2, 3].

Various acidic or base catalysts have been investigated for the depolymerization of PA-6: the organocatalyst dimethylaminopyridine [4], *p*-toluenesulphonic acid [5], sodium hydroxide [6], and sulfuric acid [2]. Recently, a lanthanide-based metal-organic catalyst showed superior activity to decompose PA-6 [7], but unfortunately this catalyst is sensitive to humidity or oxygen, requiring vacuum conditions. As a promising alternative to the above materials, heteropoly acids (HPA) are a specific type of acids which pose high solubility in water, high thermal stability, and stronger acidity than common mineral acids, i.e., H_2SO_4 or HCl.

[1]Axel Schultheis, [1]Dr. Vico Tenberg,
[2]Prof. Liisa Rihko-Struckmann, [2]Prof. Kai Sundmacher,
[1]apl. Prof. Heike Lorenz (lorenz@mpi-magdeburg.mpg.de)
[1]Physical and Chemical Foundations of Process Engineering Group, Max Planck Institute for Dynamics of Complex Technical Systems, Sandtorstr. 1, 39106 Magdeburg, Germany.
[2]Process System Engineering Group, Max Planck Institute for Dynamics of Complex Technical Systems, Sandtorstr. 1, 39106 Magdeburg, Germany.

Furthermore, the heteropoly acids are non-toxic, easy to synthesize, and sustainable in terms of creating a low amount of waste during the synthesis [8]. They are especially applicable for hydration reactions due to their tunable acidic and redox multifunctionality [9]. Chemically seen, these polyoxometallates are clusters of transition metal oxoanions linked by shared oxygen atoms resulting in a three-dimensional structure. The structure can be fine-tuned on molecular or atomic level influencing on the acidic properties, redox ability, and acid-redox-bifunctionality. HPAs can be used dissolved in water (homogeneous) or immobilized on heterogeneous supports, e.g., on silica, metal oxide supports, carbon or metal organic frameworks [9]. One example of HPAs is tungstophosphoric acid (TPA, $H_3PW_{12}O_{40}$), a super acid in aqueous solutions. TPA solutions were successfully used for cellulose decomposition [10–12].

TPA is also promising for the depolymerization of PA-6. Chen et al. used the TPA to accelerate the hydrolysis of PA-6 under hydrothermal conditions in the temperature range of 280 to 330 °C [13]. They observed that the main product is CPL, whereas byproducts such as 6-aminocaproic acid and its dimer, trimer, tetramer, and pentamer and oligomers of CPL were also identified.

In the depolymerization of PA-6 catalyzed by TPA the reactor effluent constitutes the desired monomeric product CPL, possible residue of the polymer and the dissolved TPA in an aqueous mixture. In the point of view for process design and recycle of the catalyst, the separation of TPA and the obtained monomer must be realized. The monomer CPL is extremely soluble in water [14, 15]. Therefore, the separation of CPL and the well water-soluble catalyst in aqueous environment poses a challenge.

For this, crystallization is an advantageous unit operation as it is commonly used to separate high-purity compounds from solutions. This would minimize the loss in product quality over the recycling process. Solid-liquid equilibria (SLE), required to properly design crystallization processes, are available for the system CPL/water, among others, in literature [14–18]. In addition to the separation of high-purity monomers, crystallization might allow for a simple recycle of the TPA catalyst in the liquid phase. Alternatively, crystallization could be preceded by a liquid-liquid extraction to separate the TPA catalyst and thus simplify the subsequent crystallization of CPL.

This work focuses on preliminary investigations to generate CPL in the depolymerization of PA-6 using TPA and the potentials and limitations of crystallization-based processes for its recovery from the reaction solution. The reactor effluent after a TPA-supported depolymerization constitutes unconverted PA-6, the monomer CPL as the preferred product, and the water-soluble catalyst TPA. The unconverted, solid PA-6 is easily removed by filtration. Recovery of CPL from the aqueous reactor effluent by extraction necessitates a solvent with favorable liquid-liquid equilibrium with water. Therefore, to create a first conception for CPL recovery, we searched for organic solvents showing largest possible partition of CPL towards the organic solvent phase in a solvent/water mixture. To support the experimental studies, solubilities of CPL in water, cyclohexanol (cHexOH), and 1-heptanol (HEP) have been determined and compared to predictions obtained using perturbed-chain statistical associating fluid theory (PC-SAFT) or the conductor-like screening model for real solvents (COSMO-RS) approach.

2 Theory

The solubility of a specific compound i in a given solvent or solvent mixture is an equilibrium property. In equilibrium, among others, partial pressure, temperature, and chemical potential of a compound are equal for all considered phases. Exemplified for the chemical potential μ in a liquid L and solid S phase in equilibrium, this yields:

$$\mu_i^L = \mu_i^S \tag{1}$$

For a pure solid phase ($x_i^S = 1$), Eq. (1) can be described as a function of the liquid phase molar fraction x_i^L, its corresponding activity coefficient γ_i^L, and the reference-state fugacities f_i^0 in both phases, Eq. (2) [19].

$$\ln\left(\frac{f_i^{0,S}}{f_i^{0,L}}\right) = \ln\left(x_i^L \gamma_i^L\right) \tag{2}$$

The ratio of reference-state fugacities can be calculated from melting properties of the pure solid of compound i using Eq. (3). Here, melting properties such as melting temperature $T_{m,i}$, molar melting enthalpy $\Delta H_{m,i}$, and molar heat capacity difference between pure solid and its melt $\Delta C_{p,m,i}$ are employed.

$$\begin{aligned}\ln\left(\frac{f_i^{0,S}}{f_i^{0,L}}\right) = &-\frac{\Delta H_{m,i}\left(T_{m,i}\right)}{RT}\left(1-\frac{T}{T_{m,i}}\right)\\ &-\frac{1}{RT}\int_{T_{m,i}}^{T}\Delta C_{p,m,i}\left(T\right)dT\\ &+\frac{1}{R}\int_{T_{m,i}}^{T}\frac{\Delta C_{p,m,i}\left(T\right)}{T}dT\end{aligned} \tag{3}$$

For simplicity, in this work, the molar heat capacity difference is calculated as the ratio of the molar melting enthalpy and melting temperature $\Delta C_{p,m,i} = \Delta H_{m,i}/T_m$.

Using Eqs. (2) and (3), the solubility x_i^L of a given solute in a solvent (-mixture) can be calculated. However, to account for non-idealities in the mixture, the activity coefficients γ_i^L need to be calculated. This work utilizes the PC-SAFT equation-of-state to determine activity coefficients, which is detailed in Sect. 2.1. To screen for possible extraction agents for a liquid-liquid extraction of CPL from aqueous solution, COSMO-RS was utilized to estimate thermodynamic partition coefficients for CPL between water and the potential extraction agents. This is further explained in Sect. 2.2.

2.1 Perturbed-Chain Statistical Associating Fluid Theory (PC-SAFT)

The PC-SAFT equation-of-state [20, 21] interprets molecules as chains of connected hard spheres, where molecular interactions are described by specific interactions between chains representing either the same or different molecules. To mathematically describe such chains, three parameters are required. These parameters are the number of chain segments m, the temperature-independent segment diameter of one segment σ, and the dispersion energy interaction $\frac{u}{k}$ between chains describing the same molecule. For associating molecules, i.e., molecules capable of forming hydrogen bonds, two additional parameters are required, describing the association energy $\frac{\varepsilon^{A_iB_i}}{k}$ and association volume $\kappa^{A_iB_i}$. Interactions between different molecules can be calculated from compound-specific parameters by using the following mixing rules, Eqs. (4) to (7) [20, 21]:

$$\left(\frac{u}{k}\right)_{ij} = \left(1 - k_{ij}\right)\sqrt{\left(\frac{u}{k}\right)_{ii}\left(\frac{u}{k}\right)_{jj}} \tag{4}$$

$$\sigma_{ij} = \frac{1}{2}\left(\sigma_i + \sigma_j\right) \tag{5}$$

$$\frac{\varepsilon^{A_iB_j}}{k} = \frac{1}{2}\left(\frac{\varepsilon^{A_iB_i}}{k} + \frac{\varepsilon^{A_jB_j}}{k}\right) \tag{6}$$

$$\kappa^{A_iB_j} = \left(\frac{\sqrt{\sigma_i\sigma_j}}{\sigma_{ij}}\right)^3 \sqrt{\kappa^{A_iB_i}\kappa^{A_jB_j}} \tag{7}$$

where k_{ij} describes the dispersion energy correction parameter between molecules i and j, which is typically fitted to experimental data sets using a simple temperature dependence, e.g., as shown in Eq. (8) [22].

$$k_{ij} = k_{ij,T_0} + k_{ij,T}\cdot\left(T - T_0\right) \tag{8}$$

Using these mixed parameters, the compressibility factor Z can be calculated as the sum of various contributions resulting from chain interactions, Eq. (9).

$$Z = 1 + Z^{hc} + Z^{disp} + Z^{assoc} \tag{9}$$

The derivation of different contributions for the hard chain Z^{hc} and dispersion Z^{disp} are given in [21], while equations for the association contribution Z^{assoc} can be found in [23]. The compressibility factor Z is subsequently used to calculate the fugacity coefficient φ using the definition of the residual chemical potential μ_i^{res}, Eq. (10) [21]. The activity coefficient can directly be determined by relating the fugacity coefficient of a given mixture to its value for pure i as shown in Eq. (11).

$$\ln\left(\varphi_i\right) = \frac{\mu_i^{res}}{kT} - \ln\left(Z\right) \tag{10}$$

$$\gamma_i = \frac{\varphi_i\left(T, P, x_i\right)}{\varphi_i^0\left(t, P, x_i = 1\right)} \tag{11}$$

2.2 Conductor-Like Screening Model for Real Solvents (COSMO-RS)

In addition to the PC-SAFT approach, we estimated computationally the thermodynamic partition of CPL in a solvent-water interface for eight candidates to identify suitable solvents. The partition coefficient $P^{w,org}$, Eq. (12) of a solute between an organic solvent and water is defined as:

$$P^{w,org} = \frac{x_{org}}{x_w} \tag{12}$$

with x_{org} and x_w being the solute mole fractions in the organic (org) and water phase (w), respectively. COSMO-RS calculation delivers the partition estimation of a compound in infinite dilution in pure solvents. The thermodynamic partition was estimated here assuming an equal volume size for both solvent phases.

The fully predictive COSMO-RS based on quantum chemistry and statistical thermodynamics can describe liquid-liquid and solid-liquid thermodynamics [24]. COSMO is a continuum solvation model and constructs the molecule surface as a cavity of charged, small surface segments. In the COSMO approach, the electrostatic charges of the surface segments are predicted by calculating the electron density. In a nonideal mixture, the charged segments of all molecules are paired, and so the chemical potentials of components are predicted. The COSMO approach is largely used in the pharmaceutic and biotechnology research to predict solubility of highly functionalized molecules [25, 26] or recently also for screening of promising ionic liquids for dissolution of typical plastic wastes [27].

In the present study, the phase equilibria predictions between the solvent and water as well as the solubility of the solute CPL in the selected solvents were performed using the software package BIOVIA COSMOthermX (Version 23.0.0) with the BP-TZVPD-FINE parametrization. The database COSMObase-1301 provided the computational information (COSMO-files) for the common solvents used in the present study.

3 Materials and Methods

3.1 Chemicals

The employed chemicals are summarized in Tab. 1. The received materials were applied without further purification. Water was purified via a Milli-Q-Advantage until it had a total carbon content of 4 ppb and an electric resistivity of 18.2 MΩ cm at 25 °C.

3.2 Experimental Procedures

3.2.1 Depolymerization Experiments

Depolymerization of PA-6 was performed in a 0.27-L stainless-steel autoclave reactor (Büchi AG, Switzerland)

Table 1. Chemicals used in this work.

Substance	CAS	Supplier	Purity/ grade	Molar mass [g mol^{-1}]
ε-Caprolactam	105-60-2	Sigma-Aldrich	99 %	113.16
Tungstophosphoric acid	12501-23-4	VWR	NORMAPUR	2880.2[a)]
Cyclohexanol	108-93-0	Sigma-Aldrich	ReagentPlus 99 %	100.16
1-Heptanol	111-70-6	ThermoScientific	99 %	116.20
Acetonitrile	75-05-8	VWT or alternative	HiPerSolv $\geq$ 99.9 %	41.05
		Merck	LiChrosolv $\geq$ 99.9 %	
Acetic acid	64-19-7	Roth	Rotipuran 100 % p.a.	60.05
Trifluoroacetic acid	76-05-1	Sigma-Aldrich	For HPLC $\geq$ 99.0 %	78.04
PA-6 Nylon Filament		Spectrumfilament.com	No 5903175651426	

a) Molar mass of the anhydrous form is given, however, an unspecified hydrate form was supplied.

equipped with an agitator. The reactor temperature (max. 300 °C) was regulated by a thermostat measuring the temperature inside the autoclave. The reactor was heated electrically, and the autonomous pressure was recorded (not controlled) during the experiments. The catalyst, TPA, was weighed and dissolved into ion-free water (Milli-Q, Merck, Germany) and PA-6 filament cuts, 10 mm length (Ø 1.7 mm) were added. The mixture of PA-6(6.6)/water (100.0)/TPA(3.0) (mass [g]) was placed into the autoclave, purged with N_2 for 10 min, and heated up to the reaction temperature of 250 °C within roughly 10 min. After reaching the desired temperature, the duration of depolymerization experiments was set to 30, 90, 150 or 270 min. After the desired reaction time, the reactor was cooled and vented before discharging. The solid polymer residue was separated by filtering paper (Whatman, 7–12 µm pore size), the aqueous reactor effluent was weighed, and the CPL concentration in the reactor effluent was measured by HPLC-RID to calculate the mass of the monomer in the effluent. The yield of CPL was calculated as follows:

$$Y_{CPL} = \frac{m_{CPL}}{m_{PA-6,init}} \cdot 100\% \quad (13)$$

3.2.2 Binary Solubility Experiments

The solubility of CPL in water was measured using a DSC-based method. For this, gas-tight 120-µL steel crucibles were employed. CPL was ground using mortar and pestle and filled into the crucibles. Then water was added, and the crucibles were closed. Total sample masses were around 30 mg, the CPL content ranged from ca. 10 to 95 wt %. Afterwards, the crucibles were inserted into a DSC3 (Mettler Toledo, Switzerland). The employed temperature program started with a heating step to 70 or 95 °C to liquefy and homogenize the sample, followed by cooling at −5 K min^{-1} to −70 or −50 °C for recrystallization. Then, the core heating run at 2.5 K min^{-1} to 85 °C followed. Afterwards, the sample was brought back to room temperature. The liquidus (solubility) temperature was derived from the dissolution effects peak maximum temperature [28].

The CPL solubility in cHexOH was analyzed based on classical isothermal experiments. CPL and cHexOH were added into 20-mL vials, which were then brought into a water bath and heated to 60 °C while getting stirred. Temperature control was realized using a Pt100 thermometer with an accuracy of ± 0.1 K. After complete dissolution of the solid, the vials were cooled to their target temperature and equilibrated for at least 48 h under stirring. Then, the stirring was stopped to allow solid particles to settle. After a waiting period of at least 24 h, liquid samples for HPLC were taken and injected into water-filled sample vials. The equilibrated suspensions are highly viscous and therefore no filters were employed. Great care was taken that only clear liquid was sampled. For solubility measurements of CPL in HEP, a slightly modified method was applied. Here, the liquid HPLC samples were dissolved in acetonitrile (ACN) due to miscibility issues in water. For temperatures higher than 25 °C the employed syringes and cannulas were preheated.

3.2.3 Generation of the Potential CPL•2H_2O Phase

In Barduhn et al. (1982) [18], an unidentified solid CPL phase was detected and we tried to replicate this phase. According to the existence region reported there, 19.52 g CPL and 10.49 g water (i.e., 65 wt % CPL) were mixed and completely dissolved. This solution was cooled to −20 °C while getting stirred at constant temperature for seven days. Subsequently, a vacuum filtration was conducted and the obtained solid swiftly analyzed via powder X-ray diffraction (PXRD). Equipment in direct sample contact during the filtration and PXRD analysis was precooled in a freezer at −20 °C.

3.2.4 Extraction Experiments

Extraction experiments of CPL from aqueous CPL/TPA solutions were conducted by producing a synthetic reactor effluent simulating the obtained yield in the depolymerization experiments, i.e., containing 3.5 wt % CPL, 2.2 wt % TPA, and 94.3 wt % water. This mixture was shaken for 3 h and then centrifuged with a relative centrifugal force of 3768 for 90 min using a Rotanta 460 R (Andreas Hettich GmbH & Co. KG, Germany) to remove formed precipitate. The clear solution was then transferred to 20-mL vials where either HEP or cHexOH in a 1:1 weight-based ratio was added.

Afterwards, in presence of a magnetic stirrer, the vials were closed, and equilibrated for 11 days at 55 °C.

After the equilibration period, the stirring was stopped and a waiting period of one day was added to allow the liquid phases to separate completely. Then, 0.1 to 0.15 g of the upper (organic) phase was removed via a preheated cannula and syringe, diluted with approximately 1 g of ACN and analyzed by HPLC. The vial including the remaining sample was then turned upside down and the same sampling method was employed for the lower phase. The lower and upper phase were again sampled with a mass of around 1 g for gravimetric analysis. For this sample no equilibration period was employed between the samples to reduce the error caused by the re-equilibration after the removal of a significant amount of solution. The gravimetric samples were dried in an explosion-proof vacuum oven under nitrogen atmosphere at 50 mbar and 40 °C and then analyzed by PXRD.

3.2.5 HPLC Analysis

The reactor effluent was analyzed with HPLC-RID in an Agilent 1260 Infinity II system with a Primesep 100 column (4.6 mm × 150 mm, 5 µm 100 Å, SIELC Technologies Inc). The analyses were performed at 30 °C using the eluent mixture water:ACN 80:20 (vol:vol) with 0.2 vol % trifluoroacetic acid added. The mobile phase was pumped at a flow rate of 1 mL min^{-1}. The injection volume and total run-time of a single sample was 20 µL and 75 min, respectively. A calibration curve for quantification of the CPL content was established with standard solutions prepared using CPL and Milli-Q water. In the experiments, the concentrations of aqueous CPL solutions ranged from 0.08 to 2.42 wt % and the sample was diluted if necessary to achieve the calibrated range.

CPL concentrations from the binary solubility and extraction experiments were quantified using a Kinetex 150 × 4.6 mm column with a particle size of 2.6 µm. The eluent was a mixture of water:ACN 80:20 (vol:vol) + 0.1 % acetic acid employed at a flow rate of 0.5 mL min^{-1} and an oven temperature of 25 °C. Due to availability, three different systems manufactured by Agilent (USA) were used and the injection volumes were adjusted according to the detector sensitivity: Agilent 1100 (10 µL), Agilent 1260 (2 µL), Agilent Prime (1 µL). Evaluation was conducted via UV absorbance at 210 nm in the Agilent 1100 and 1260. Due to the increased sensitivity of the Agilent Prime, 230 nm were employed in this case. CPL calibration was realized by dissolving different amounts of CPL in water or ACN and correlating the measured area with the corresponding mass fraction. The retention time of CPL was around 4 min.

3.2.6 PXRD Analysis

Solids were analyzed by PXRD using a X'Pert Pro diffractometer (PANalytical GmbH, Germany). CuKα radiation was employed and a 2θ range from 5 to at least 30° with a resolution of 0.017° and a measuring time of 50 s per step. Temperature-resolved PXRD measurements were conducted with a heating rate of 1 K min^{-1} (up to 95 °C) or 5 K min^{-1} (up to 250 °C) at isothermal steps after an equilibration time of 3 min. Analysis was performed from 5 to 30° with a resolution of 0.017° and a measuring time of 45 s.

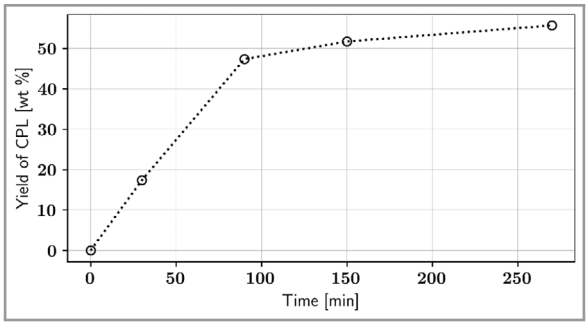

Figure 1. Yield of CPL (Eq. (13)) as a function of the reaction time at the reaction temperature 250 °C. Obtained CPL amount measured in the reactor effluent.

4 Results and Discussion

4.1 Depolymerization

TPA catalyzed the depolymerization of the polyamide, PA-6. Fig. 1 illustrates the influence of the reaction time on the CPL yield, e.g., a yield of CPL was 47.3 % at a reaction time of 90 min. An extension of the reaction time to 150 and 270 min increased the yield slightly further. However, complete depolymerization of PA-6 was not achieved, and the yield of CPL remained below 56.0 % under all investigated conditions.

From the depolymerization experiments one could conclude that TPA is a highly active catalyst for PA-6 depolymerization. Our results are in line with CPL yields obtained at slightly higher temperatures (280 °C to 330 °C) by Chen et al [13]. However, using the water-soluble TPA as catalyst, the reactor effluent is an aqueous mixture of the desired product CPL and the TPA catalyst. At a yield of 55.7 %, as obtained at the reaction time of 270 min, assuming no losses in filtering and complete removal of PA-6, absence of side products, and fully soluble TPA, the aqueous reactor effluent is composed of 3.5/2.2/94.3 (wt %) for CPL, TPA, and water, respectively.

4.2 COSMO-RS Predictions

Tab. 2 lists the computationally predicted thermodynamic partition coefficients of CPL for a few solvents. The computationally predicted values are useful to rank various solvents and to select two solvent candidates for experimental separation studies. As seen in Tab. 2, the partition of CPL

Table 2. COSMO-RS-predicted thermodynamic partition coefficients and mass fraction solubilities of CPL in various solvents at 25 °C.

Solvent	Partition coefficient, $P^{w,org}$	CPL solubility, w_{CPL}
Cyclohexanol (cHexOH)	4.786	0.476
1-Heptanol (HEP)	4.835	0.425
Cyclohexanone	1.374	0.367
Benzene	0.441	0.373
Toluene	0.319	0.213
n-Heptane	0.021	0.007
Cyclohexane	0.020	0.008
Water	–	0.896

in cHexOH/water and HEP/water systems was estimated to be advantageous for the conception of the CPL separation.

The mass fraction solubility w_{CPL} of CPL in the solvents and in water was predicted by the COSMO-RS approach as well (see Tab. 2). The predicted solubility of CPL in water is in line with experimental data ($w_{CPL} \approx 0.85$ at 25 °C (see Sect. 4.4). The solubility of CPL in organic solvents depends on the polarity of the solvent, and this trend was clearly observed in the computational predictions as well. Very low CPL solubility was predicted for the nonpolar solvents, e.g., cyclohexane and *n*-heptane. At the same time, the predicted solubility of CPL in polar solvents, e.g., in cHexOH and HEP, is higher than that in nonpolar ones. The computational predictions by COSMO-RS were used here to rank various solvents. Therefore, the polar solvents cHexOH and HEP were selected for the experimental crystallization measurements, as a high partition coefficient indicates a preferred, high extraction efficiency.

4.3 PXRD Analysis of ε-Caprolactam and TPA

Measured PXRD patterns of CPL and TPA in comparison to data obtained from the CCDC and ICSD are displayed in Figs. 2 and 3. Our measured diffractogram of CPL, as presented in Fig. 2, is in good accordance with [29]. At least four hydrates of TPA are known [30–33]. Ground samples of TPA were analyzed by temperature-resolved PXRD, Fig. 3, showing mainly that a solid-state transformation takes place between room temperature and 40 °C. For the original TPA material no good PXRD signal but rather small and broad peaks, thus a low peak-to-baseline ratio was observed. No reference fitted to our data. At 30 °C three different, but similar patterns were obtained. The measurement at 40 °C shows peaks from a hexahydrate described in [31] and additional ones, indicating a mixture of two hydrate forms of TPA. At 175 °C the pattern corresponds well to the hexahydrate [31]. The solid-state behavior is complex due to the existence of many known (and potentially unknown) TPA hydrates and due to possible temperature- or moisture-induced hydrate changes occurring. From the temperature-resolved PXRD, we conclude that TPA can lose or gain crystal water even at conditions near room temperature. Therefore, we expect that the sample at room temperature was a mixture of anhydrous and different unspecified hydrates of TPA. This behavior of TPA

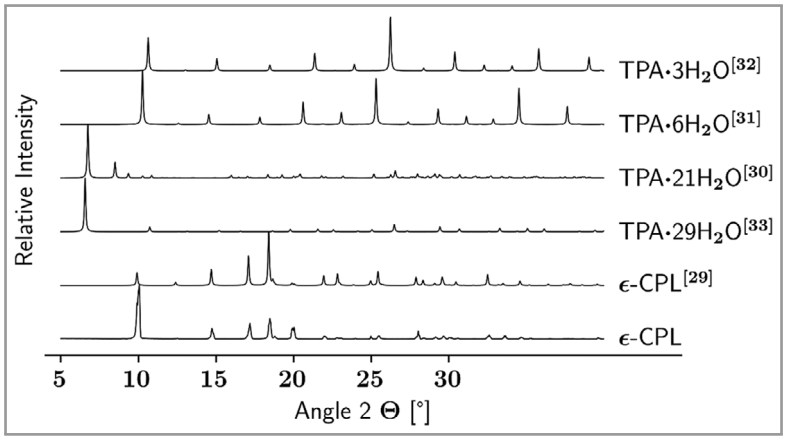

Figure 2. PXRD patterns of TPA and CPL from selected literature references and own measurement of CPL.

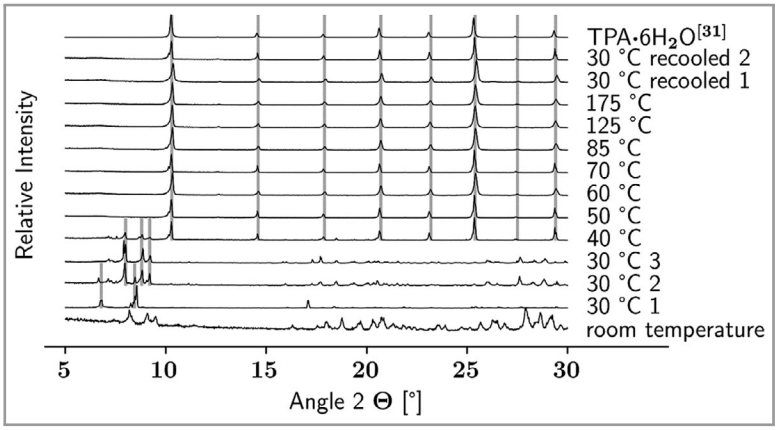

Figure 3. Temperature-resolved PXRD pattern of TPA in comparison to a TPA hexahydrate from [31], starting with a pattern of the original sample from the substance bottle (lowest PXRD pattern, room temperature). Note that for three TPA samples from the same batch three similar but different patterns were obtained at 30 °C. Beginning at 40 °C, peaks from the hexahydrate are visible. Reflexes which appear in more than one sample are marked in grey.

Table 3. Component-specific PC-SAFT parameters used in this work.

Component	m	σ [Å]	$\frac{u}{k}$ [K]	$\frac{\varepsilon^{A_iB_i}}{k}$ [K]	$\kappa^{A_iB_i}$	Ref.
CPL	4.0737	3.3551	335.37	1623.00	0.00399	[34]
Cyclohexanol	2.5278	3.9355	326.28	3010.54	0.00067	[35]
1-Heptanol	3.1788	4.0059	286.27	2916.94	0.00257	[36]
Water	1.2047	a)	353.94	2425.67	0.04510	[37]

a) $\sigma = 2.7927 + 10.11 \cdot \exp(-0.01775 \cdot T) - 1.417 \cdot \exp(-0.01146 \cdot T)$

and the numerous amounts of crystal water possible renders the usage of PXRD for the identification of solid phases challenging.

4.4 Binary Solubility of ε-Caprolactam

To obtain a basic understanding of the phase behavior of CPL, binary solubility studies in cHexOH, HEP, and water were conducted. Solid-liquid equilibria of CPL and water were previously determined and reported in literature, e.g., in [14–18], and their results are used as validation for experimental procedures within this work. Further, in [34], vapor-liquid equilibria of CPL and water were successfully modeled using the simplified PC-SAFT equation-of-state and following, pure component parameters of CPL are obtained from this study. However, since now outdated component-specific parameters of water were used, the dispersion energy correction parameter k_{ij} will be refitted in this work using more recent water-specific parameters. Similarly, since no k_{ij} values between CPL and cHexOH or HEP are reported in literature at the time of writing, they are fitted here as well. Tab. 3 shows the PC-SAFT parameters used in this work. For all associating compounds, a 2B association scheme and number of association sites $N_{assoc} = 2$ was assumed.

To estimate the dispersion energy correction parameters k_{ij} between CPL and the solvents, only the lowest and highest solubility value were considered. From this, k_{ij} values of $0.0096 - 0.0013(T[\mathrm{K}] - 298.15\ \mathrm{K})$, -0.0317, and -0.0987 were obtained for CPL in cHexOH, HEP, and water, respectively. Melting temperature of 342.3 K and molar melting enthalpy of 16096 J mol^{-1} of CPL were obtained from literature [38, 39].

As described in Sect. 3.2, due to high solubility and viscosity, solid-liquid equilibria were determined via DSC measurements. In literature, solubility determination via DSC measurement was already proven to be a promising alternative to classical equilibria experiments [40]. Solubilities of CPL in cHexOH and HEP were determined with classic isothermal methods. Fig. 4 shows the solubility of CPL in water, cHexOH, and HEP as a function of temperature, cHexOH and HEP exhibit an overall lower solubility for CPL, e.g., of ~ 27 wt % and ~ 46 wt % at 25 °C, respectively, as opposed to ~ 84 wt % in water. At 55 °C, solubilities in cHexOH and HEP increase to ~ 83 wt % and ~ 80 wt %, respectively. Using model parameters from literature (see Tab. 3) and the aforementioned regressed binary dispersion energy correction parameters, PC-SAFT is able to describe the different solvents sufficiently accurate. Additionally, the dashed blue line shows the prediction of the CPL solubility in water with outdated water-specific parameters as used in [34]. While these parameters showed good agreement with vapor-liquid equilibria between water and CPL, the prediction utilized in this work exhibits a significant improvement for the description of solid-liquid equilibria, especially with decreasing temperatures.

From the measured CPL/water solid-liquid equilibria, presented in Fig. 4 and later in Fig. 9, it is observed that the eutectic or peritectic composition (in case of metastable or stable equilibria (see Fig. 9)) are located above 60 wt % CPL, which need to be surpassed to allow for solid CPL to be precipitated. In a potential process however, typical CPL concentrations might be lower (< 5 wt %) and thus water would crystallize as ice prior to solid CPL. Therefore, to allow CPL to directly crystallize from this solution, large fractions of water are required to be evaporated, decreasing the economic viability of the process. As an alternative, CPL could be separated from the TPA catalyst via a liquid-liquid extraction coupled with subsequent crystallization of CPL from the organic phase. Additionally, this would allow for an easy recycle of the utilized catalyst. Based on COSMO-RS predictions, cHexOH and HEP were considered as liquid-liquid extraction agents and their CPL solubility was investigated to design a crystallization from a binary system (see Sect. 4.2).

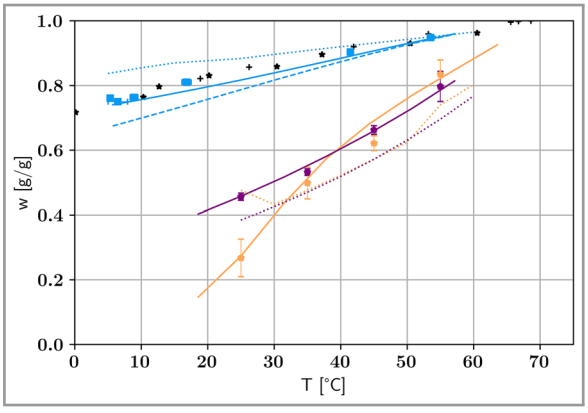

Figure 4. Measured solubility of CPL in water, cyclohexanol, and 1-heptanol. Blue squares: solubility in water via DSC; orange pentagons: in cHexOH and purple pentagons: in HEP via isothermal experiments. Error bars represent the standard deviation of a sample. Solid lines denote calculated solubilities via PC-SAFT with the current parameters, while the dashed lines indicate outdated parameters. Literature data for the solubility of CPL in water is represented by black symbols: +: [15], ∗: [14].

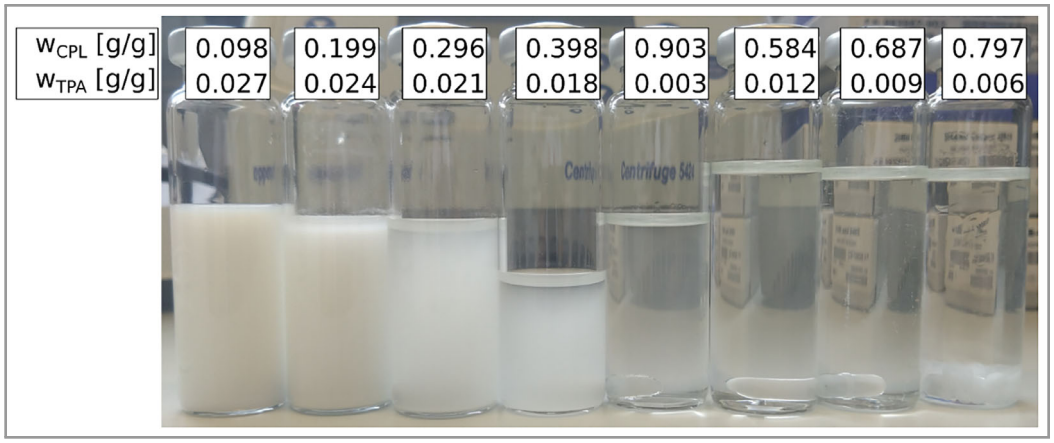

Figure 5. Mixtures of CPL with an aqueous 3 wt % TPA solution. The resulting weight fractions of CPL and TPA are given in the figure. Note the white precipitation appearing at lower concentrations.

4.5 Unknown Precipitation in the CPL/TPA/Water System

As Sect. 4.4 focuses on simple binary CPL/solvent systems, in a real process the presence of the TPA catalyst will influence the phase behavior and the solubility of CPL and thus needs to be investigated prior to the process design. As discussed in Sect. 4.1, the TPA/water ratio during the depolymerization experiments was 3/97 (wt/wt) and was not adjusted for the experiments in this section. In an effort to measure the solubility of CPL in the presence of TPA, several mixtures of varying CPL content in the TPA/water mixture were prepared. Upon mixing, white precipitate was observed in several samples (see Fig. 5). Unintuitively, lower concentrations of CPL lead to increased precipitation. This is especially unexpected as the TPA and CPL concentrations were much lower than their pure solubility in just water.

The precipitates were analyzed by PXRD (see Fig. 6) and revealed numerous reflexes of which we could attribute a few to mainly the TPA patterns at 30 °C. Interestingly, CPL was not encountered in significant amount. We could not clarify the origin of the remaining peaks up to now but consider that they might belong to hydrate forms of TPA. As our goal is crystallizing CPL from the reaction mixture, we here assume that this precipitate is fully separated from the solution during the filtration step, which is used to separate the unreacted polymer after the depolymerization.

4.6 CPL/Water Phase Behavior and Phase Diagram

In [18], an unknown solid phase based on CPL was reported. To clarify the phase behavior in this region of the phase diagram, additional experiments were conducted, as described in Sect. 3.2.3, to obtain the so far unknown phase. The resulting diffraction pattern is displayed in Fig. 7. It exhibits distinctive peaks of CPL in addition to new peaks indicated by the gray bars. Consequently, two distinct solid phases were present in the sample. A possible reason for

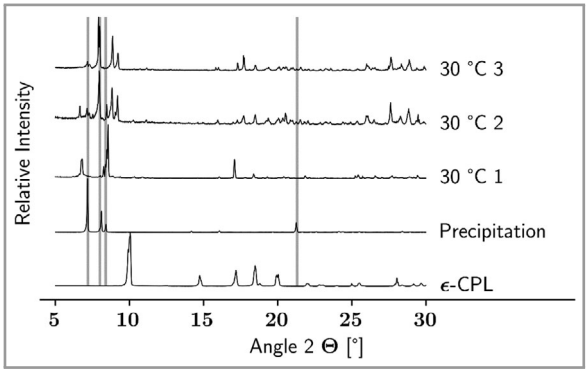

Figure 6. Diffractograms of a solid from an aqueous mixture initially containing 9.8 wt % CPL and 2.7 wt % TPA. The reflexes from the obtained precipitation correspond partly to the measured TPA references at 30 °C as indicated by the grey bars.

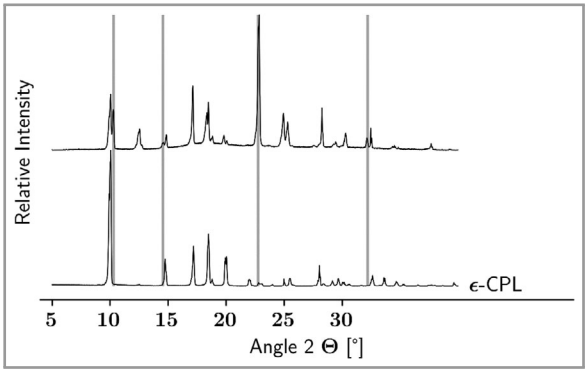

Figure 7. Diffractogram of the obtained solid after cooling the CPL/water solution to −20 °C compared to the CPL pattern. Note the reference reflexes from CPL and additional ones marked in grey.

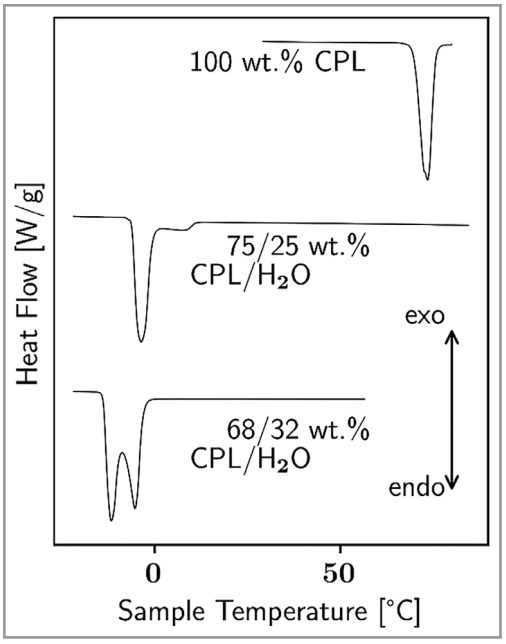

Figure 8. DSC curves of CPL and 75/25 and 68/32 wt % CPL/H_2O mixtures. Only the heating runs without recrystallization effects are shown. The CPL melting curve was measured without pre-homogenization step and was scaled for better presentability.

the observation of CPL could be partial phase transition of the obtained low-temperature phase to the pure CPL phase at ambient conditions during PXRD analysis as the equipment was not cooled during measurement and thus a temperature increase in the sample occurred. Alternatively, metastability of the secondary solid phase would explain its transition to CPL. Nevertheless, the second solid phase, which could not be identified as a previously reported CPL-based phase, agrees with the results reported in [18]. Following the phase behavior illustrated in Fig. 9, it needs to be a hydrate phase of CPL; its initial composition close to the molar 1:2 CPL:H_2O ratio points to a CPL·2H_2O phase.

To further clarify the phase behavior, additional DSC studies were performed to derive the full melt phase diagram of the CPL/H_2O system. The measurement details are given in Sect. 3.2.2 and were also used to determine the CPL solubility in water at higher CPL contents. The additional measurements thus referred to lower CPL contents and, for assignment of the new solid phase, to the related intermediate composition range. Exemplary DSC heating runs of CPL and samples of 68/32 and 75/25 wt % CPL/water mixtures are depicted in Fig. 8.

DSC heating runs at several cases revealed various thermal events such as melting and recrystallization phase transitions. To facilitate the comparison of different sharp peaks caused by invariant points in the phase diagram, the peak onset temperature was taken for those events. As mentioned in Sect. 3.2.2, liquidus temperatures were determined from the peak maximum temperatures of the related dissolution effects. Sharp endothermic peaks followed by an exothermic event indicate melting of a phase followed by recrystallization of a new one, e.g., due to incomplete phase transition or mixing issues in the sample preparation/homogenization steps.

For the CPL/H_2O system, the temperatures of various thermal effects are illustrated in Fig. 9 as a function of the CPL content, representing the related phase diagram. There, stable equilibria are indicated by solid lines and metastable equilibria by dashed lines. Eutectic and peritectic invariants in the CPL/H_2O system were found, whereby the eutectic at the lowest temperature of −19.6 °C turned out to be metastable regarding a stable one at −13.5 °C and a peritectic at −6.6 °C occurring due to the presence of an intermediate hydrate phase of 1:2 CPL:H_2O ratio already indicated above. Its existence and stoichiometry is confirmed by the DSC results in the related composition region (compare Fig. 8), clearly revealing the presence of the eutectic phase transition at −13.5 °C below and the peritectic one at −6.6 °C above its characteristic 1:2, i.e., 75.8 wt % composition

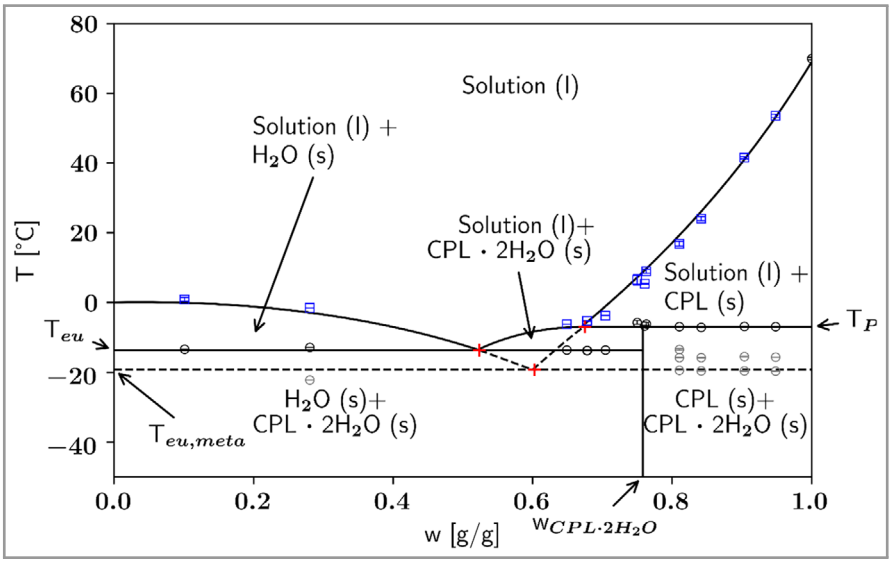

Figure 9. Phase diagram of the CPL/H_2O system, with the CPL content given in total mass fraction. O, □: experimental DSC measurements of this work; red crosses: invariant points published in [18]. Blue squares represent solubilities in the system. Black lines characterize stable phase equilibria specified by black circles; dashed lines: metastable equilibria indicated by grey circles. Lines are used to guide the eye based on the invariant points determined in [18]. Error bars are given as standard deviation of a sample.

Table 4. CPL mass fractions of equilibrated aqueous and organic phases after extraction at 55 °C. Additionally, the corresponding thermodynamic partition coefficients, $K_{D,ex}$, calculated as $\frac{w_{CPL,org}}{w_{CPL,aq}}$ based on experimental results are given.

Extraction agent	$w_{CPL,aq}$	$w_{CPL,org}$	$K_{D,ex}$
HEP	0.011 ± 0.001	0.020 ± 0.002	1.9 ± 0.4
HEP ref[a)]	0.0997	0.1776	1.8
cHexOH	0.008 ± 0.002	0.023 ± 0.005	3.1 ± 1.4

a) Experiments were performed at 60 °C, in a ternary system containing only CPL, HEP, and water [41].

(see Fig. 9). The invariant temperatures and compositions determined agree very well with those reported before [18]. Obviously, the reason that the compound was not described previously can be attributed to the challenges working at strongly sub-zero temperature conditions.

4.7 Liquid-Liquid Extraction

As stated in Sect. 4.4, it might be advantageous to utilize liquid-liquid extraction and subsequent crystallization from an organic solvent as opposed to direct crystallization from the aqueous reaction mixture to purify CPL. Based on the COSMO-RS prediction, shown in Tab. 2, cHexOH and HEP were chosen as extraction agents, and their efficacy is validated in this section. Therefore, aqueous mixtures of CPL and TPA were prepared and extracted via cHexOH or HEP as described in Sect. 3.2.4. After equilibration of the two liquid phases at 55 °C, both phases were sampled and analyzed via HPLC. The resulting CPL contents are listed in Tab. 4.

Overall, the experimentally determined partition coefficients show an enrichment of CPL in the organic phase. Experimental results using HEP are well comparable to results in [41] measured at 60 °C without TPA (see Tab. 4). The experimental partition coefficient for cHexOH is with 3.08 ± 1.4 much higher than expected and connected with a high standard deviation. Thus, further experimental investigations should be conducted to reduce the standard deviation of this specific result. In both organic phases, TPA was not found via PXRD after complete evaporation of the liquid. As CPL is enriched in HEP and cHexOH, both organic solvents show potential as extraction agents. At this stage one should note that the values of the measured partition coefficients presented in Tab. 4 and the by COSMO-RS predicted values in Tab. 2 are not directly comparable due to the assumptions done during COSMO-RS calculations (infinite dilution of the solute in pure solvent phases, no mutual miscibility of the phases, and equal phase volumes).

Additionally, as previously discussed in Sect. 4.4, both solvents exhibit reduced CPL solubility and an increased temperature dependence on solubility as compared to water as a solvent. This makes both solvents promising candidates for a hybrid process of liquid-liquid extraction with subsequent crystallization of CPL from organic solution.

5 Conclusion

Potential purification processes for the separation of CPL from a depolymerization reaction mixture were discussed in this study. For this, a depolymerization of PA-6 with a TPA catalyst in aqueous solution was performed resulting in a 47.3 % yield for a reaction time of 90 min at 250 °C. Two separation strategies of CPL from the reaction mixture, ideally consisting of CPL, TPA, and water, were proposed: direct crystallization of CPL or prior liquid-liquid extraction and subsequent CPL crystallization from organic phases.

To gauge the efficacy of the investigated separation methods, solubilities of CPL in water, cHexOH, and HEP were measured. cHexOH and HEP were chosen as promising extraction agents based on calculated thermodynamic partition coefficients, derived for water and various organic solvents with COSMO-RS calculations. From the three investigated solvents, at 25 °C, water exhibited the highest solubility for CPL with ∼ 84 wt %, followed by HEP (∼ 46 wt %), and finally cHexOH (∼ 27 wt %). These solubilities were additionally modeled via PC-SAFT, where component-specific model parameters were obtained from literature with the dispersion energy correction parameters k_{ij}, which were fitted to our experimental values. The results exhibited good agreement between the experimental and modeled data sets.

Via DSC-based solubility determination in the CPL/water system, a dihydrate phase of CPL was found, which means that CPL can only be obtained at CPL contents exceeding the peritectic composition at 67.5 wt % CPL and crystallization temperatures above the peritectic temperature of −6.6 °C. As the aqueous reaction mixture contains a maximum of 6.2 wt % CPL, assuming 100 % conversion from PA-6, a direct crystallization from the reaction mixture is not feasible, as upon cooling, water would crystallize. To allow for CPL crystallization, large amounts of water need to be evaporated or removed, e.g., via membranes [42], to reach the mentioned domain below the solubility curve of CPL (see Fig. 9).

In addition to the high energy demand for water evaporation, water also exhibits very high solubility for CPL, decreasing the potential yield of its subsequent crystallization. It should be added here that after potential CPL concentration melt crystallization can be an alternative for high-purification of CPL, which was not investigated in this work. However, a promising approach is a liquid-liquid extraction with cHexOH and HEP. Experimental partition coefficients were 3.1 ± 1.4 and 1.9 ± 0.4 for cHexOH and HEP, respectively. Both organic solvents exhibit similar extraction performance, however, cHexOH is the more promising candidate for the subsequent crystallization due to lower solubility and stronger temperature dependence of the solubility. While attempting to measure CPL solubilities in aqueous TPA solutions, white precipitation was observed that could not be attributed to CPL, leading to

the hypothesis that TPA precipitated in the prepared mixtures. After the depolymerization, this would not have been observed as the unreacted polymer is removed via filtration, which likely removed the unknown precipitate as well.

Apart from the investigations of a potential purification process, the overall phase behavior of CPL and water was investigated via DSC and PXRD measurements. A previously undefined solid phase reported in [18] could be assigned to an incongruently melting CPL·2H_2O compound in the CPL/H_2O phase diagram connected with a peritectic phase transition in the system. However, further experimental work is required to confirm the 1:2 stoichiometry gravimetrically, which is hampered by the sub-zero temperature conditions needed and the particular nucleation and recrystallization phenomena in the system.

This work lays the foundation for future investigation and process design for the complete depolymerization of PA-6 and purification of CPL monomers from the aqueous solution or by subsequent liquid-liquid extraction followed by crystallization. Additional efforts should focus on screening depolymerization reaction conditions, in particular alternative catalysts avoiding TPA, and potential extraction agents. Independent on the catalyst finally chosen, its recycling needs to be considered for further process design.

Acknowledgment

This work was partly supported by the Research Initiative "SmartProSys: Intelligent Process Systems for Sustainable Production of Chemicals" funded by the Ministry for Science, Energy, Climate Protection and the Environment of the State of Saxony-Anhalt, Germany. It was further supported by the Deutsche Forschungsgemeinschaft (DFG, German Research Foundation) under grant number 501735683. Open Access funding was provided by the Max Planck Society. We thank Surini Hansika Nishshanka Pathirennahalage for support in experimental investigations and Jacqueline Kaufmann and Stefanie Oberländer for their continuous support in the lab work.

Open access funding enabled and organized by Projekt DEAL.

Author Contribution

Axel Schultheis: Methodology, validation, formal analysis, investigation, visualization, writing – original draft

Vico Tenberg: Methodology, modeling, validation, formal analysis, investigation, visualization, writing – original draft

Liisa Rihko-Struckmann: Methodology, modeling, validation, formal analysis, investigation, writing – original draft

Kai Sundmacher: Writing – review and editing, resources, funding acquisition

Heike Lorenz: Conceptualization, supervision, writing – original draft, review and editing, resources, funding acquisition

Symbols used

C_p	[J mol^{-1}K^{-1}]	molar heat capacity
f	[Pa]	fugacity
H	[J mol^{-1}]	molar enthalpy
k_{ij}	[–]	dispersion energy correction parameter
m	[g]	mass
m	[–]	segment number
P/K	[–]	thermodynamic partition coefficient (P: mole-based; K: weight-based)
T	[K]	temperature
u/k	[K]	dispersion energy parameter
w	[g^{-1}]	weight fraction
x	[mol mol^{-1}]	mole fraction
Y	[wt %]	yield
Z	[–]	compressibility factor

Greek letters

ε/k	[K]	association energy parameter
φ	[–]	fugacity coefficient
γ	[–]	activity coefficient
κ	[–]	association volume parameter
μ	[J mol^{-1}]	chemical potential
σ	[Å]	segment diameter

Abbreviations

ACN	acetonitrile
cHexOH	cyclohexanol
COSMO-RS	conductor-like screening model for real solvents
CPL	ε-caprolactam
HEP	1-heptanol
PA-6	polyamide-6
PC-SAFT	perturbed-chain statistical associating fluid theory
PXRD	powder X-ray diffraction
SLE	solid-liquid equilibria
TPA	tungstophosphoric acid

References

[1] I. Vollmer, M. J. F. Jenks, M. C. P. Roelands, R. J. White, T. van Harmelen, P. de Wild, G. P. van der Laan, F. Meirer, J. T. F.

Keurentjes, B. M. Weckhuysen, *Angew. Chem., Int. Ed.* **2020**, *59* (*36*), 15402–15423. DOI: https://doi.org/10.1002/anie.201915651
[2] A.-J. Minor, R. Goldhahn, L. Rihko-Struckmann, K. Sundmacher, *Chem. Eng. J.* **2023**, *474*, 145333. DOI: https://doi.org/10.1016/j.cej.2023.145333
[3] V. Hirschberg, D. Rodrigue, *J. Polym. Sci.* **2023**, *61* (*17*), 1937–1958. DOI: https://doi.org/10.1002/pol.20230154
[4] C. Alberti, R. Figueira, M. Hofmann, S. Koschke, S. Enthaler, *Chem. Select.* **2019**, *4* (*43*), 12638–12642. DOI: https://doi.org/10.1002/slct.201903970
[5] S. P. Khuntia, A. Gadgeel, S. Mestry, S. T. Mhaske, *Polym. Adv. Technol.* **2022**, *33* (*1*), 411–426. DOI: https://doi.org/10.1002/pat.5526
[6] X.-H. Chen, G. Wu, S.-C. Chen, Y.-Z. Wang, *Polymer* **2023**, *283*, 126201. DOI: https://doi.org/10.1016/j.polymer.2023.126201
[7] L. Wursthorn, K. Beckett, J. O. Rothbaum, R. M. Cywar, C. Lincoln, Y. Kratish, T. J. Marks, *Angew. Chem., Int. Ed.* **2023**, *62* (*4*), e202212543. DOI: https://doi.org/10.1002/anie.202212543
[8] X. Luo, H. Wu, C. Li, Z. Li, H. Li, H. Zhang, Y. Li, Y. Su, S. Yang, *Front Chem*. **2020**, *8*. DOI: https://doi.org/10.3389/fchem.2020.580146
[9] L. Hombach, N. Simitsis, J. T. Vossen, A. J. Vorholt, A. K. Beine, *ChemCatChem* **2022**, *14* (*12*). DOI: https://doi.org/10.1002/cctc.202200616
[10] K. Shimizu, H. Furukawa, N. Kobayashi, Y. Itaya, A. Satsuma, *Green Chem*. **2009**, *11* (*10*), 1627. DOI: https://doi.org/10.1039/b913737h
[11] P. Lanzafame, D. M. Temi, S. Perathoner, A. N. Spadaro, G. Centi, *Catal. Today* **2012**, *179* (*1*), 178–184. DOI: https://doi.org/10.1016/j.cattod.2011.07.018
[12] B. Meryemoglu, *Catal. Commun*. **2021**, *149*, 106248. DOI: https://doi.org/10.1016/j.catcom.2020.106248
[13] J. Chen, Z. Li, L. Jin, P. Ni, G. Liu, H. He, J. Zhang, J. Dong, R. Ruan, *J. Mater. Cycles Waste Manage.* **2010**, *12* (*4*), 321–325. DOI: https://doi.org/10.1007/s10163-010-0304-y
[14] X. Gong, Y. Lü, G. Luo, *Chin. J. Chem. Eng.* **2010**, *18* (*2*), 286–291. DOI: https://doi.org/10.1016/S1004-9541(08)60354-7
[15] R. Puffr, *Collect. Czech. Chem Commun.* **1969**, *34* (*5*), 1421–1428. DOI: https://doi.org/10.1135/cccc19691421
[16] P. J. Diepen, O. S. L. Bruinsma, G. M. V. Rosmalen, *Chem. Eng. Sci.* **2000**, *55* (*18*), 3575–3584. DOI: https://doi.org/10.1016/S0009-2509(00)00044-0
[17] M. Poschmann, *Zu den Nachbehandlungsschritten der Suspensionskristallisation aus Schmelzen, Thesis*, Universität Bremen **1995**.
[18] A. J. Barduhn, M. Handley, *J. Chem. Eng. Data* **1982**, *27* (*3*), 306–308. DOI: https://doi.org/10.1021/je00029a022
[19] *Molecular Thermodynamics of Fluid-Phase Equilibria* (Eds.: J. M. Prausnitz, R. N. Lichtenthaler, E. G. de Azevedo), Pearson Education **1998**.
[20] J. Gross, G. Sadowski, *Ind. Eng. Chem. Res.* **2002**, *41* (*22*), 5510–5515. DOI: https://doi.org/10.1021/ie010954d
[21] J. Gross, G. Sadowski, *Ind. Eng. Chem. Res.* **2001**, *40* (*4*), 1244–1260. DOI: https://doi.org/10.1021/ie0003887
[22] H. T. Do, Y. Z. Chua, A. Kumar, D. Pabsch, M. Hallermann, D. Zaitsau, C. Schick, C. Held, *RSC Adv*. **2020**, *10* (*72*), 44205–44215. DOI: https://doi.org/10.1039/D0RA08947H
[23] W. G. Chapman, K. E. Gubbins, G. Jackson, M. Radosz, *Ind. Eng. Chem. Res.* **1990**, *29* (*8*), 1709–1721. DOI: https://doi.org/10.1021/ie00104a021
[24] A. Klamt, *J. Phys. Chem.* **1995**, *99* (*7*), 2224–2235. DOI: https://doi.org/10.1021/j100007a062
[25] L. König-Mattern, S. Linke, L. Rihko-Struckmann, K. Sundmacher, *Green Chem*. **2021**, *23* (*24*), 10014–10029. DOI: https://doi.org/10.1039/D1GC03471E
[26] I. W. Cordova, G. Teixeira, P. J. A. Ribeiro-Claro, D. O. Abranches, S. P. Pinho, O. Ferreira, J. A. P. Coutinho, *Ind. Eng. Chem. Res.* **2024**, *63* (*21*), 9565–9575. DOI: https://doi.org/10.1021/acs.iecr.4c00652
[27] M. Mohan, J. D. Keasling, B. A. Simmons, S. Singh, *Green Chem*. **2022**, *24* (*10*), 4140–4152. DOI: https://doi.org/10.1039/D1GC03464B
[28] H. Lorenz, Solubility and Solution Equilibria in Crystallization, in Crystallization, Basic Concepts and Industrial Applications (Ed.: W. Beckmann), Wiley-VCH, Weinheim, Wiley **2013**, 35–74.
[29] F. K. Winkler, J. D. Dunitz, *Acta Crystallogr. B* **1975**, *31* (*1*), 268–269. DOI: https://doi.org/10.1107/S0567740875002440
[30] M.-R. Spirlet, W. R. Busing, *Acta Crystallogr. B* **1978**, *34* (*3*), 907–910. DOI: https://doi.org/10.1107/S0567740878004306
[31] J. Haber, L. Matachowski, D. Mucha, J. Stoch, P. Sarv, *Inorg. Chem*. **2005**, *44* (*19*), 6695–6703. DOI: https://doi.org/10.1021/ic050350s
[32] L. Marosi, E. Escalona Platero, J. Cifre, C. Otero Areán, *J. Mater. Chem.* **2000**, *10* (*8*), 1949–1955. DOI: https://doi.org/10.1039/b001476l
[33] A. J. Bradley, J. W. Illingworth, *Proc. R. Soc. London, Ser. A* **1936**, *157* (*890*), 113–131. DOI: https://doi.org/10.1098/rspa.1936.0183
[34] I. A. Kouskoumvekaki, G. J. P. Krooshof, M. L. Michelsen, G. M. Kontogeorgis, *Ind. Eng. Chem. Res.* **2004**, *43* (*3*), 826–834. DOI: https://doi.org/10.1021/ie034082m
[35] C. Coquelet, C.-B. Soo, A. Valtz, D. Richon, D. Amoros, H. Gayet, *Fluid Phase Equilib*. **2010**, *298* (*1*), 33–37. DOI: https://doi.org/10.1016/j.fluid.2010.06.013
[36] V. Pokorný, V. Štejfa, M. Klajmon, M. Fulem, K. Růžička, *J. Chem. Eng. Data* **2021**, *66* (*1*), 805–821. DOI: https://doi.org/10.1021/acs.jced.0c00878
[37] L. F. Cameretti, G. Sadowski, *Chem. Eng. Process. Process Intensif.* **2008**, *47* (*6*), 1018–1025. DOI: https://doi.org/10.1016/j.cep.2007.02.034
[38] A. A. Kozyro, L. I. Marachuk, A. P. Krasulin, I. A. Yursha, G. Y. Kabo, *Zh. Prikl. Khim. (Leningrad)* **1989**, *62*, 595.
[39] G. J. Kabo, A. A. Kozyro, V. S. Krouk, V. M. Sevruk, I. A. Yursha, V. V. Simirsky, V. I. Gogolinsky, *J. Chem. Thermodyn.* **1992**, *24* (*1*), 1–13. DOI: https://doi.org/10.1016/S0021-9614(05)80249-6
[40] R. Mohan, H. Lorenz, A. S. Myerson, *Ind. Eng. Chem. Res.* **2002**, *41* (*19*), 4854–4862. DOI: https://doi.org/10.1021/ie0200353
[41] M. Wijtkamp, G. H. van Bochove, T. W. de Loos, S. H. Niemann, *Fluid Phase Equilib*. **1999**, *158–160*, 939–947. DOI: https://doi.org/10.1016/S0378-3812(99)00124-7
[42] L. Zhang, P. Yu, Y. Luo, *Sep. Purif. Technol.* **2006**, *52* (*1*), 77–83. DOI: https://doi.org/10.1016/j.seppur.2006.03.020

